



Modelling and correcting the impact of RF pulses for continuous monitoring of hyperpolarized NMR

Gevin von Witte^{1,2}, Matthias Ernst², and Sebastian Kozerke¹

¹University and ETH Zurich, Institute for Biomedical Engineering, Zurich 8092, Switzerland

²ETH Zurich, Laboratory of Physical Chemistry, Zurich 8093, Switzerland

Correspondence: Sebastian Kozerke (kozerke@biomed.ee.ethz.ch)

Abstract. Monitoring the build-up or decay of hyperpolarization in nuclear magnetic resonance requires radio-frequency (RF) pulses to generate observable nuclear magnetization. However, the pulses also lead to a depletion of the polarization and, thus, alter the spin dynamics. To simulate the effects of RF pulses on the polarization build-up and decay, we propose a first-order rate-equation model describing the dynamics of the hyperpolarization process through a single source and a relaxation term.

5 The model offers a direct interpretation of the measured steady-state polarization and build-up time constant. Furthermore, the rate-equation model is used to study three different methods to correct for the errors introduced by RF pulses: (i) a $1/\cos^n \theta$ correction, which is only applicable to decays, (ii) an analytic formula to correct for the build-up and decay times and (iii) a newly proposed iterative, self-consistent correction. The corrections are first tested in low signal-to-noise ratio (SNR) simulations (SNR around 40 for 2.5° pulses), predicting accurate results ($\pm 10\%$ error) up to 25° pulses. The correction methods are

10 then tested on experimental data obtained with dynamic nuclear polarization (DNP) using 4-oxo-TEMPO in ^1H glassy matrices, resulting in high SNR acquisitions (around 1000 for 2.4° pulses). It is experimentally demonstrated that the rate-equation model allows to obtain build-up times and steady-state polarization (enhancement) even for large RF flip angles (25°) during build-up yielding results within $\pm 10\%$ error when compared to data acquired with small RF flip angles ($< 3^\circ$). For decay experiments, corrections are shown to be accurate for up to 12° RF flip angles with discrepancies to the simulations attributed to

15 the low experimental acquisition SNR. In conclusion, corrections based on a rate-equation description offer fast and accurate estimations of achievable polarization levels and build-up time constants in hyperpolarization experiments for a wide range of samples.

1 Introduction

20 Improving the sensitivity of nuclear magnetic resonance (NMR) through hyperpolarization methods (Ardenkjaer-Larsen et al., 2015; Kovtunov et al., 2018; Akbey et al., 2013; Corzilius, 2020) requires an understanding of the limiting processes and, hence, accurate experimental measurements and data. In dynamic nuclear polarization (DNP), repeated radio-frequency (RF)



pulses are applied to measure build-up and decay times as well as steady-state polarization. However, the readout RF pulses necessary to measure the polarization levels alter the state of the spin system by converting some of the polarization into detectable transverse magnetization. The larger the RF pulses, the stronger the z-magnetization is affected by the measurement process and with this the time evolution of the system. This leads to changes in the experimentally determined parameters compared to the undisturbed situation where no RF pulses are applied. The effect of RF pulses can be minimized by using small flip-angle pulses with long repetition times or by repeating DNP experiments with a single large flip-angle pulse applied at the end of the individual experiment. The former approach often leads to noisy data and, hence, to poor estimates of the build-up time constant and steady-state polarization, whereas the latter is time consuming. We investigate an intermediate path with repeated pulses of variable flip angles and repetition times. We correct for the effect of the readout RF pulses on the spin dynamics, leading to more accurate and faster measurements.

The manuscript is divided into two parts. First, different RF correction methods are investigated in simulations including a rate-equation model consisting of a single polarization source and a relaxation term. Second, the simulated RF correction approaches are tested experimentally on data obtained with DNP in glassy ^1H matrices containing 4-oxo-TEMPO. Together, the theoretical foundation for the correction of RF pulse effects in hyperpolarized NMR and its practical feasibility are presented, allowing the use of larger flip angles to obtain more accurate measurements of the experimental quantities of interest.

2 Theory: Rate-equation model

Let us consider a system that includes a hyperpolarization source and a relaxation term. For the source, we start from Fermi's golden rule and assume that the injected polarization is proportional to the available density of states, with the rate constant given by k_W . The total density of states is denoted by A , the occupied states by the nuclear polarization P and, hence, the available density of states is given by $(A - P)$. The relaxation is characterized by the relaxation-rate constant k_R . In the following, we ignore the thermal-equilibrium polarization as it is typically small compared to the polarization generated by the hyperpolarization process, e.g., enhancements $\epsilon = \frac{P_{\text{hyp}}}{P_{\text{eq}}}$ of more than 100 are often reported (Ardenkjær-Larsen et al., 2003; Jähnig et al., 2017; Leavesley et al., 2018; Ni et al., 2013; Corzilius, 2020; Rej et al., 2015; Kwiatkowski et al., 2018a; Shimon et al., 2022; Yoon et al., 2019; Dementyev et al., 2008; Hope et al., 2021; Jardón-Álvarez et al., 2020). Combining the above arguments, the rate equation for the polarization is given by

$$\frac{dP}{dt} = (A - P) \cdot k_W - k_R \cdot P \quad (1)$$

In the following, k_W will be referred to as the (DNP) polarization injection rate as we describe the model based on the experimental setup of DNP. However, it can also be adopted for spin-exchange optical pumping (SEOP) (Walker and Happer, 1997), para-hydrogen based techniques (Natterer and Bargon, 1997; Adams et al., 2009; Kovtunov et al., 2018), triplet DNP in pentacene crystals as polarization sources for target solutions (Tateishi et al., 2014; Miyanishi et al., 2021; Eichhorn et al., 2022) or nitrogen-vacancy (NV) centers in diamond to hyperpolarize surface or bulk spins in diamond (King et al., 2015; Broadway et al., 2018; Ajoy et al., 2018; Miyanishi et al., 2021).



55 Here, A describes the total density of states which are accessible for building up nuclear hyperpolarization P . In DNP, the
magnitude of A would be determined by the thermal electron polarization as this governs the maximally possible enhancement.
In spin-exchange optical pumping (SEOP), A would be given by the polarization of alkali atoms under circular-polarized laser
irradiation (Walker and Happer, 1997), in para-hydrogen-based techniques, such as para-hydrogen-induced hyperpolarization
(PHIP) or signal amplification by reversible exchange (SABRE), by the initial polarization level of the para-hydrogen molecules
60 (Natterer and Bargon, 1997; Adams et al., 2009; Kovtunov et al., 2018).

The mechanism of (DNP) polarization injection can be a complex problem as it not only involves the initial quantum-
mechanical polarization transfer from the electron to a hyperfine-coupled nucleus but also strong paramagnetic relaxation and
the transport of the created nuclear polarization from the nuclei close to the electron (local nuclei) into the bulk as discussed
in (Prisco et al., 2021). This spin transport might be drastically slowed down due to paramagnetic shifts of the local nuclei
65 compared to the bulk. This aspect, often called spin-diffusion barrier, has recently received renewed interest (Smith et al.,
2012; Wittmann et al., 2018; Wenckebach et al., 2021; Tan et al., 2019; Stern et al., 2021; Chessari et al., 2022). Our rate-
equation model largely ignores these microscopic complications by describing the polarization injection as a single step that
builds up the polarization.

Solving Eq. (1) leads to

$$70 \quad P(t) = \frac{Ak_W}{k_W + k_R} \cdot \left(1 - e^{-(k_W + k_R)t}\right) \quad (2)$$

which can be compared to an experimentally used Ansatz of the form

$$P_{\text{exp}}(t) = P_0 \cdot (1 - e^{-t/\tau_{\text{bup}}}) \quad (3)$$

to find a correspondence between the parameters in our theoretical model and the phenomenological experimental description.

For steady-state polarization P_0 and the build-up time constant τ_{bup} one obtains

$$75 \quad P_0 = \frac{Ak_W}{k_W + k_R} = Ak_W \tau_{\text{bup}} \quad (4a)$$

$$\tau_{\text{bup}}^{-1} = k_W + k_R \quad (4b)$$

and

$$k_W = \tau_{\text{bup}}^{-1} \frac{P_0}{A} \quad (5a)$$

$$k_R = \tau_{\text{bup}}^{-1} \left(1 - \frac{P_0}{A}\right) \quad (5b)$$

80 For an identical relaxation-rate constant k_R , a smaller injection parameter k_W would lead to longer build-up times and lower
enhancements. For a value of k_W much larger than k_R the steady-state polarization would approach A and the build-up
time would be a measure of the injection parameter. However, this scenario is rarely observed experimentally and would
represent the ideal case. For rather small experimental polarizations with respect to A , the build-up time would be similar to
the relaxation-rate constant. We note that similar expressions for the steady-state polarization and build-up time have been
85 derived in (Smith et al., 2012; Corzilius et al., 2012) for coupled nuclear-electron rate-equation systems.



The model described above only requires three parameters to describe the build-up dynamics: A , k_W and k_R . The value of A is determined by experimental conditions, e.g. in DNP by the thermal electron polarization which depends mostly on the magnetic field and temperature. The rate constants k_W and k_R can be deduced from the measured build-up time constant and the steady-state polarization as indicated in Eqs. (5a, 5b).

90 Eliminating the injection (source) term from Eq. 2 or setting k_W to zero, leaves only the relaxation term remaining. This corresponds to a decay experiment which is described by a simple exponential decay $P_{\text{exp,d}}(t) = P_0' \cdot e^{-t/\tau_{\text{decay}}}$. The solution of the differential equation is straightforward and the decay time constant is given by

$$\tau_{\text{decay}}^{-1} = k_R \quad (6)$$

The initial polarization in the decay case is given by the polarization that was created during the hyperpolarization build-up.
95 We would like to stress that the relaxation-rate constant during the decay does not have to be the same as during the build-up since the experimental conditions may not be the same. For example, the microwave irradiation in DNP is turned on during the build-up but typically switched off during the decay.

In the following, the proposed rate-equation model is studied in simulations using a time slicing algorithm with RF pulses depleting the polarization repeatedly. Different methods to correct for the effects of RF pulses on the hyperpolarization dynamics
100 are investigated theoretically before being tested experimentally.

3 Theory: Radio-frequency pulse correction

To investigate the effects of repeated RF pulses on the magnetization and the polarization dynamics, we integrate Eq. (1) and apply RF pulses (with flip angle θ) at a fixed repetition time T_R . To avoid confusion, we do not specify a time unit in our simulations as different samples can have widely different time scales experimentally, e.g., ^1H DNP with 4-oxo TEMPO builds
105 up in tens of seconds (see experimental results below), ^{13}C DNP in diamond through the endogenous P1 centers takes tens of minutes (Kwiatkowski et al., 2018a) and silicon nano- and microparticles take hours (Dementyev et al., 2008; Kwiatkowski et al., 2018b). Fig. 1a shows simulated build-ups under different RF readout schemes relative to a reference simulation without pulses. Stronger pulses or shorter repetition times lead to apparently reduced build-up times and steady-state polarizations as shown in Fig. 1a and Tab. 1.

θ	[°]	2.5	2.5	7	12.5	25
T_R	[a.u.]	2	1	2	2	2
τ_{bup}	[a.u.]	48.9	47.8	42.2	31.3	14.5
P_0		0.293	0.287	0.254	0.190	0.091

Table 1. Fitted build-up times of noiseless simulated data **1** under the influence of different RF schemes (compare Fig. 1a). Assumed experimental parameters without pulses: $P_0 = 0.3$, $\tau_{\text{bup}} = 50$, $A = 1$.

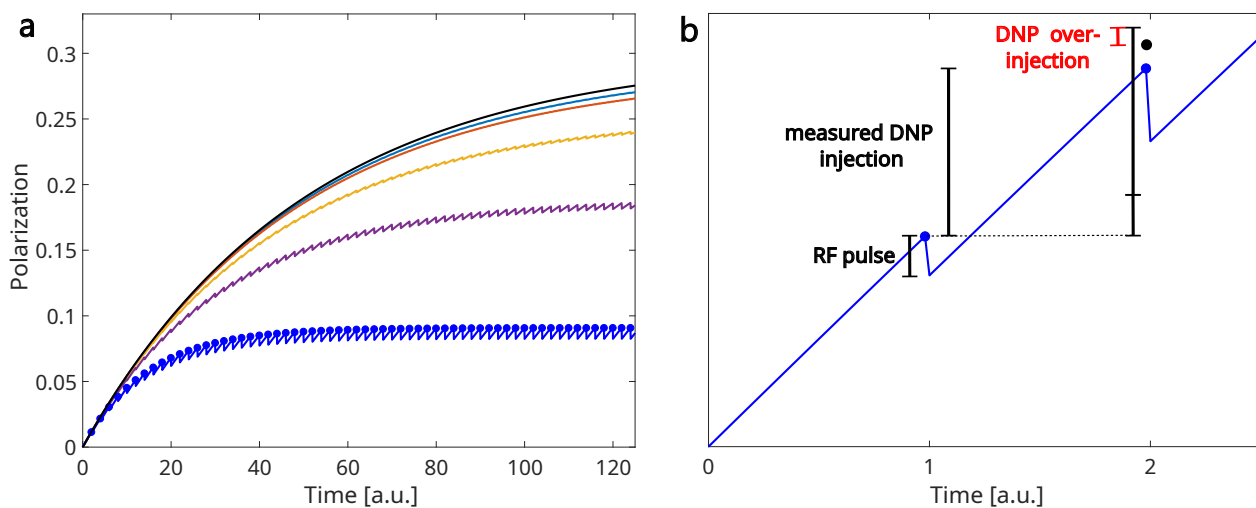


Figure 1. (a) Comparison of simulated build-ups under the influence of RF pulses (see text for details). The black curve is without RF pulses. The RF scheme for the other curves (from top to bottom): 2.5°, 2 time units; 2.5°, 1 time unit; 7°, 2 time units; 12.5°, 2 time units; 25°, 2 time units. Assumed experimental parameters without pulses: $P_0 = 0.3$, $\tau_{\text{bup}} = 50$, $A = 1$. (b) Illustration of RF correction during build-up. The blue points indicate the measured polarization. The black point indicates the true polarization in the absence of RF pulses. Note that the first data point is exact without any RF correction. The blue line shows the polarization in the presence of RF pulses, DNP injection and relaxation. An increased signal due to DNP injection is observed from the first to the second data point. The RF pulse decreases polarization.

110 Correcting for the effects of RF pulsing during a build-up requires us to consider three aspects as outlined in Fig. 1b: (i)
 The measured polarization might change between consecutive data points as the steady-state is not yet reached, (ii) a readout
 RF pulse reduces the polarization while the polarization is assumed to be unaffected ($M_{xy} = \sin(\theta)M_z$) and (iii) the reduced
 polarization leads to a weaker effect of relaxation and a stronger effect of polarization injection.

115 In the following, an iterative correction algorithm is proposed that takes the measured data as input and corrects for the effects
 of the repeated RF pulses. The first two terms of the correction algorithm describe the measured polarization difference between
 consecutive data points and the correction for the depletion by an RF pulse. The third contribution, which we call Δ_{n-1} for
 the n -th acquired data point, describes the DNP overinjection due to the changes in polarization given the $(n-1)^{\text{th}}$ RF pulse.
 In the following, we will denote the measured polarization without any correction with P_n and the corrected polarization with
 \tilde{P}_n , equal to the theoretical, RF-free experiment. The DNP overinjection Δ_{n-1} is given by



$$\begin{aligned}
 120 \quad d\tilde{P}_{n-1} &= \left[(A - \tilde{P}_{n-1}) \cdot k_W - k_R \cdot \tilde{P}_{n-1} \right] \cdot dt \\
 dP_{n-1} &= \left[(A - \cos(\theta) \cdot P_{n-1}) \cdot k_W - k_R \cdot \cos(\theta) \cdot P_{n-1} \right] \cdot dt \\
 \Rightarrow \Delta_{n-1} &= (\tilde{P}_{n-1} - \cos(\theta) \cdot P_{n-1}) \cdot \underbrace{(k_W + k_R)}_{\tau_{\text{bup}}^{-1}} dt
 \end{aligned} \tag{7}$$

and with this we can write an iterative correction

$$\begin{aligned}
 \tilde{P}_n &= \tilde{P}_{n-1} + \underbrace{(P_n - P_{n-1})}_{\text{DNP injection}} + \underbrace{(\cos(\theta)^{-1} - 1) \cdot \cos(\theta) \cdot P_{n-1}}_{\text{RF pulse}} \\
 125 \quad &- \underbrace{(\tilde{P}_{n-1} - \cos(\theta) \cdot P_{n-1}) \cdot (k_W + k_R) \cdot T_R}_{\text{DNP overinjection through RF depleted polarization } (\Delta_{n-1})} \\
 &= \tilde{P}_{n-1} + (P_n - \cos(\theta) P_{n-1}) \\
 &- (\tilde{P}_{n-1} - \cos(\theta) \cdot P_{n-1}) \cdot (k_W + k_R) \cdot T_R
 \end{aligned} \tag{8}$$

This iterative correction algorithm works accurately in simulations of noise-free and noisy data as shown in Fig. 2.

We use the definition of the build-up time constant from Eq. (4b) as already indicated in Eq. (7). However, correcting the
 130 experimental data with the measured build-up time leads to a different build-up time after the first correction step. Hence, a self-consistent iterative algorithm first fitting the build-up time and then using it to correct the data is implemented. This scheme of correcting the data and fitting the updated data is continued until either a predefined maximum number of iterations (500) is exceeded or the change between successive iterations is below a threshold (1e-4 s).

Extension to the decay case is straightforward as only the build-up time needs to be replaced by the decay time constant in
 135 the correction.

4 Methods

All simulations and corrections were implemented in Matlab (Mathworks, Natick, MA). The self-consistent correction as described in the previous Section is compared to two other correction approaches: First, $1/\cos^n \theta$, with n being the number of RF pulses, is used to correct for depletion through readout RF pulses during decay. Second, if only the build-up or decay time
 140 constant is of interest, a simple model presented in the supplementary information of Capozzi et al. (2017) can be used. The true build-up time constant τ_{bup} (or alternatively the decay time constant τ_{decay}) can be calculated according to

$$\tau_{\text{bup}} = \left(\frac{1}{\tau'} + \frac{\ln(\cos(\theta))}{T_R} \right)^{-1} \tag{9}$$

with τ' being the measured time constant without correction for RF pulses. This approach considers RF pulsing being an external relaxation channel that needs to be compensated for. As the model was introduced by Capozzi and Comment et al. we
 145 will refer to it as the CC-correction in the following.



All experimental data were acquired with 50mM 4-oxo-TEMPO in water/glycerol mixtures using DNP. In particular, we compare two different sample formulations with TEMPO in DNP juice (6:3:1 mixture of glycerol- d_8 , D_2O and H_2O) or TEMPO in $(1/1)_V H_2O/$ glycerol (no deuteration, all protonated). After mixing the ingredients, the filled sample container was frozen in liquid nitrogen before being transferred to a cryogenically pre-cooled polarizer (cryostat temperature during the transfer below 20K).
150

The protonated sample formulation was reported to show a mono-exponential build-up in our 7 T set-up (299 MHz 1H Larmor frequency) (Jähnig et al., 2019). In addition, fast proton spin diffusion and a homogenous radical distribution should ensure a homogenous mono-exponential build-up and decay of the polarization. Compared to our previously published work, we upgraded the system to a new microwave source (200 mW, Virginia Diodes Inc., USA) and silver-plated the wave-guides to reduce resistive losses, giving us approximately eight times more microwave power as before at the sample space (around 65 mW) (Himmler et al., 2022). Details of the experimental set-up can be found elsewhere (Jähnig et al., 2017; Himmler et al., 2022).
155

The NMR measurements were performed at a sample temperature of 3.3 K with a Bruker Avance III HD (Bruker BioSpin AG, Switzerland) spectrometer. We use a prescan delay of 18 μs to protect the spectrometer from signal overflows. All data processing was performed using Matlab scripts.
160

5 Results

5.1 Simulations

Upon introduction of noise (see discussion for experimental to simulation noise comparison) in the simulations, the iterative correction becomes gradually less accurate for larger and more repeated pulses as shown in Fig. 2. More details on the simulated performance of the corrections can be found in the Supplementary Information, section S1 for build-ups and in section S2 for decays. The CC-correction gives the most accurate time constants (see Figs. S5 and S12). However, the CC-algorithm only yields time constants and neither steady-state polarization nor individual data point correction. We note that our iterative and the CC-correction perform better on data during decays than for data acquired during build-ups when using large RF pulse angles. The $1/\cos^n$ correction performs similarly to the other two methods for data acquired during decays except for the largest flip angles simulated owing to the low SNR involved (see Discussion).
165
170

5.2 Experiment

To test these simulation results, we performed a range of build-up and decay experiments with different RF schemes to test the performance of iterative and CC-correction for the build-up and decay as well as the $1/\cos^n$ correction for the decay. Build-ups acquired with different flip angles are shown in Fig. 3a together with an example of the iterative correction and a simulation of the rate equation model confirming the validity of our approach. The input parameters of the simulated build-up are derived from the experimentally measured steady-state polarization and build-up time constant with Eqs. (5a,5b). Parameter A was
175

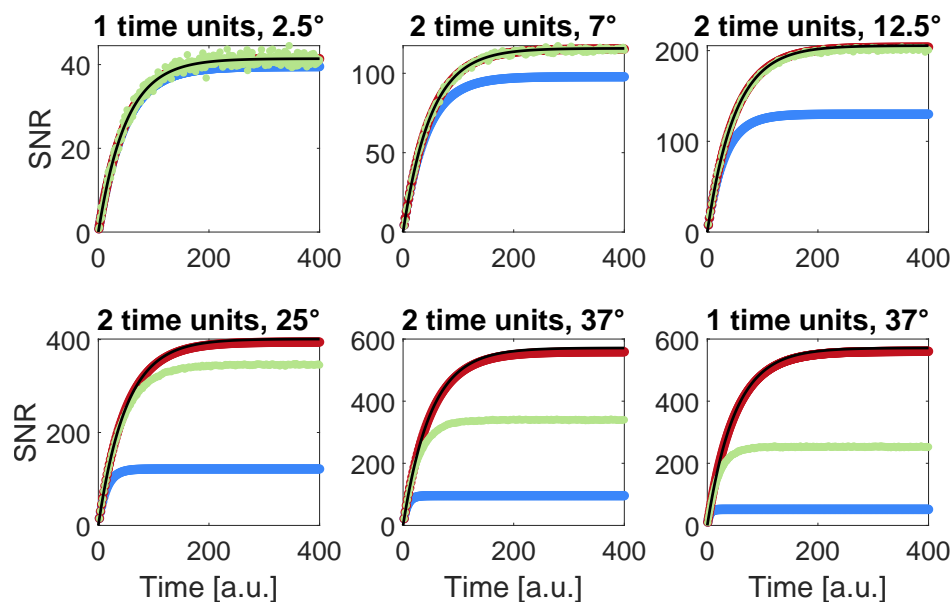


Figure 2. Simulated performance of the iterative correction: build-ups for different flip angles and repetition times with (blue) and without (black) RF pulses depleting the polarization (compare Fig. 1). Correction of the RF-depleted polarization with (green, see discussion for comparison between experimental and assumed noise in the simulations) and without (red) noise in the simulations. Assumed experimental parameters without pulses: $P_0 = 0.3$, $\tau_{\text{bup}} = 50$, $A = 1$.

set to the thermal electron polarization of 89%. The estimated relaxation rate of 0.024s^{-1} for the build-up was much larger than the measured decay relaxation rate of 0.006s^{-1} . A typical decay measurement before and after correction for RF pulses is shown in Fig. 3b.

180 The results for all measurements with TEMPO in DNP juice are summarized in Tab. 2 and Fig. 4. The respective data sets in the protonated sample are shown in Tab. 3 and Fig. 5, described by an RF relaxation rate, given by $\sin(\theta)/T_R$.

6 Discussion

In our work it has been demonstrated that the proposed rate-equation model allows us to obtain build-up times and steady-state polarization for large RF flip angles (25°) during ^1H (TEMPO in water/glycerol) polarization build-ups yielding results
185 with $\pm 10\%$ error compared to data acquired with small RF flip angles ($< 3^\circ$). Based on simulations with added noise (see Supplementary Information, sections S1 and S2 for build-up and decay, respectively), we expected the corrections to become inaccurate for too large flip angles (and relaxation-rates). Interestingly, the correction worked well for all build-up measurements up to 25° for which the simulations already started to become inaccurate. Experimentally, the corrections become
190 inaccurate for build-ups acquired with flip angles between 25 and 37° . For decays, corrections fail earlier - depending on the relaxation-rate constant between 12 and 25° . The lower accuracy of the decay can be attributed to a combination of reasons:



	θ	T_R	$\sin(\theta)/T_R$	ϵ	ϵ	τ_{bup}	τ_{bup}	τ_{bup}	τ_{decay}	τ_{decay}	τ_{decay}	τ_{decay}
	[°]	[s]	[10^{-2} s^{-1}]	uncorr.	iter. corr.	[s]	[s]	[s]	[s]	[s]	[s]	[s]
						uncorr.	iter. corr.	CC	uncorr.	iter. corr.	CC	cos. corr.
1	0.7	5	0.25	139	139	31	31	31	173	173	173	173
2	0.7	2	0.64	139	139	31	31	31	172	174	174	173
3	0.7	1	1.3	138	139	30	30	30	167	170	170	170
4	0.7	0.5	2.5	138	139	30	30	30	166	170	170	170
5	1.5	2	1.3	132	132	30	30	30	167	172	172	171
6	1.5	1	2.7	131	132	30	30	30	161	171	171	170
7	1.5	0.5	5.3	129	132	29	30	30	152	171	171	169
8	2.4	5	0.85	131	132	31	31	31	171	176	176	176
9	2.4	2	2.1	129	131	30	30	30	162	175	175	173
10	2.4	1	4.3	127	130	29	30	30	149	172	172	169
11	2.4	0.5	8.5	124	130	29	30	30	131	173	173	167
12	4.7	2	4.1	125	131	29	30	30	135	175	174	169
13	4.7	1	8.2	119	130	27	30	30	110	175	175	163
14	4.7	0.5	16	109	130	25	30	30	80	176	176	150
15	7.1	2	6.2	29	127	27	30	30	105	177	176	162
16	7.1	1	12	26	127	24	29	29	75	178	178	147
17	7.1	0.5	25	22	126	20	29	29	48	194	184	109
18	12.2	2	11	24	124	22	29	29	60	189	189	130
19	12.2	1	21	19	124	18	29	29	36	203	190	73
20	12.2	0.5	42	14	125	13	29	30	20	235	267	7
21	24.7	2	21	13	112	12	27	30	20	149	469	$6.56 \cdot 10^5$
22	24.7	1	42	8	123	8	31	33	11	737	-375	$4.93 \cdot 10^5$

Table 2. Overview of different experimental flip angles and correction methods with TEMPO in DNP juice. The iterative correction refers to the above introduced self-consistent correction algorithm. The label "CC" refers to Eq. (9), introduced by Capozzi, Comment and co-workers. For the decay, we compare these two with a simple $1/\cos^n$ correction. ϵ refers to the DNP enhancement. $\sin(\theta)/T_R$ can be interpreted as a relaxation rate due to RF pulsing. This data is summarized in Fig. 4.

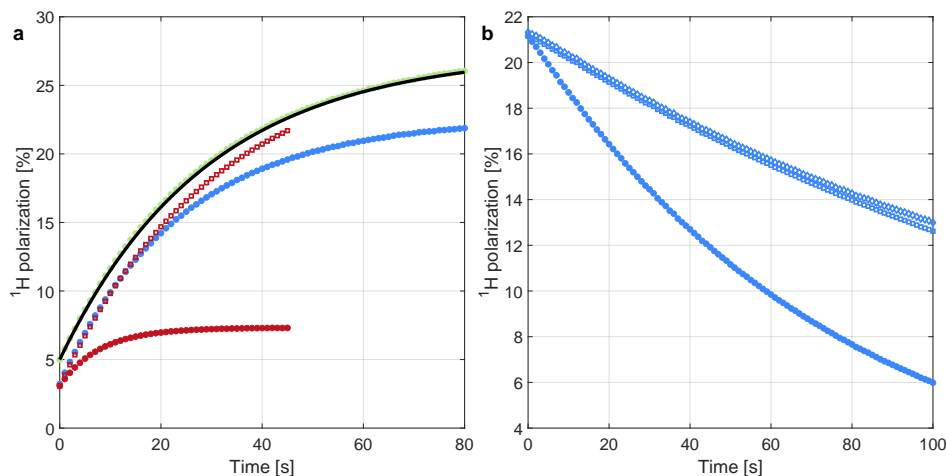


Figure 3. (a) Uncorrected experimental build-ups with different flip angles: 2.4° , 7° and 25° in green, blue and red (filled dots, see experiments 10, 16 and 22 in Tab. 2 for more details), respectively. The open red squares correspond to the 25° measurement after applying the above introduced iterative correction. For the 2.4° measurement, the corresponding build-up simulation based on the thermal electron polarization $A = 0.89$, measured steady-state polarization and build-up time is shown (see Eqs. (1.5a) and (5b)). For the first data point of the simulation, the starting polarization is set to the first experimental data point as this initial polarization is an artefact of the measurement process (see discussion for details). (b) The uncorrected decay under pulses with a flip angle of 7° every 1 s (exp. 16 in Tab. 2) is shown with filled dots and the iterative as well as $1/\cos^n$ correction in open square and diamond symbols, respectively.

(i) once the RF relaxation-rate constant becomes much larger than the thermal relaxation rate, only few data points can be acquired to estimate the thermal rate as the hyperpolarization is decaying fast; (ii) during the build-up, strong RF relaxation is not the only contribution to the system dynamics as the (DNP) injection term gets larger due to the low polarization under pulsing. When the two reach a balance, the internal system dynamics is still important. In the decay case, the only large term dominating every other process is the RF relaxation, rendering the thermal relaxation a small perturbation; (iii) the decay measurement starts with a low initial polarization as the strong RF relaxation (large $\sin(\theta)/T_R$) caused the polarization at the end of the build-up to be small (we performed build-up and decay in one experiment). This limits the number of data points with sufficient SNR for the overall decay fit to only a few as the polarization is very quickly depleted due to RF pulses.

The $1/\cos(\theta)^n$ correction works well for high SNR decay measurements (see Figs. S7 and S13) but cannot be used for the build-ups due to its divergent nature of the correction factor. Furthermore, for low SNR decays, the results are inaccurate as the correction factor acts only on a single data point and amplifies the noise. The other two correction approaches use all data points.

The noise added in our simulations is relatively large compared to the noise in our experiments. In the simulations a 2.5° pulse yielded an SNR of around 40 (see Fig. 2) while experimentally the SNR based on the first point of the FID is around 1000 (see Fig. S14) for a 2.4° FID of the natural abundance sample despite the long prescan delay and short T_2^* as a result of the stronger nuclear dipolar interactions, resulting in lower SNR compared to the DNP juice sample. The corrections

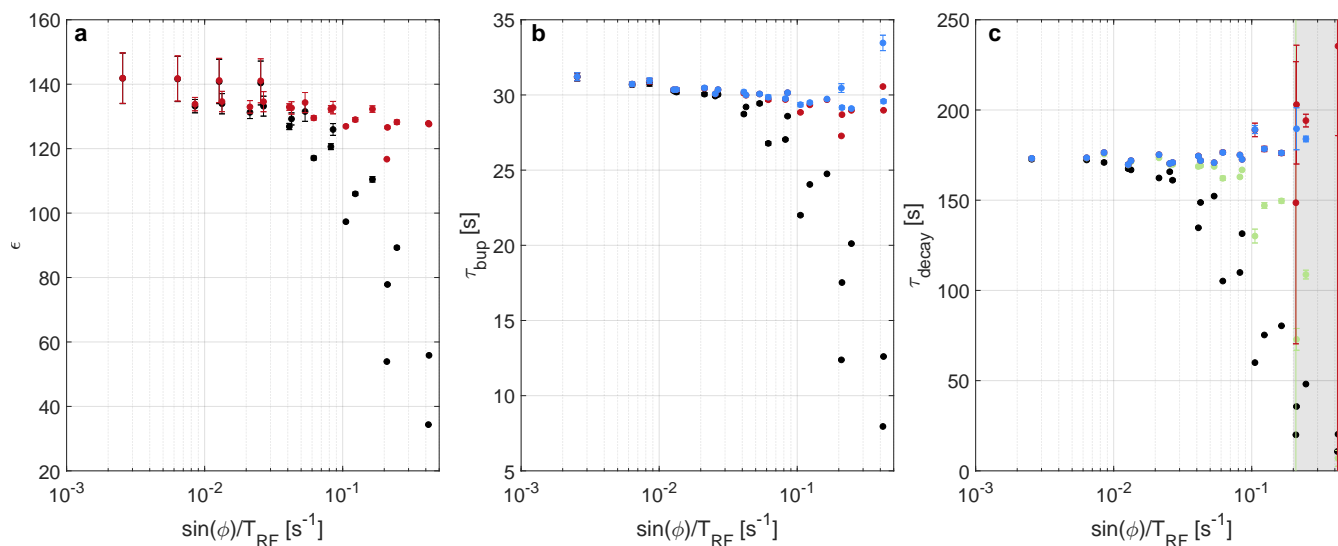


Figure 4. Experimental parameters - enhancement (a), build-up (b) and decay times (c) - with and without correction for the different experiments with TEMPO in DNP juice as shown in tab. 2, ordered by the relaxation due to RF pulsing ($\sin(\theta)/T_R$). Black refers to the uncorrected data, red to the iterative correction, blue and green to the CC-correction and $1/\cos^n$ correction, respectively. The uncertainties extracted from the 95% fit intervals of the respective build-up and decay measurements are often smaller than the symbol.

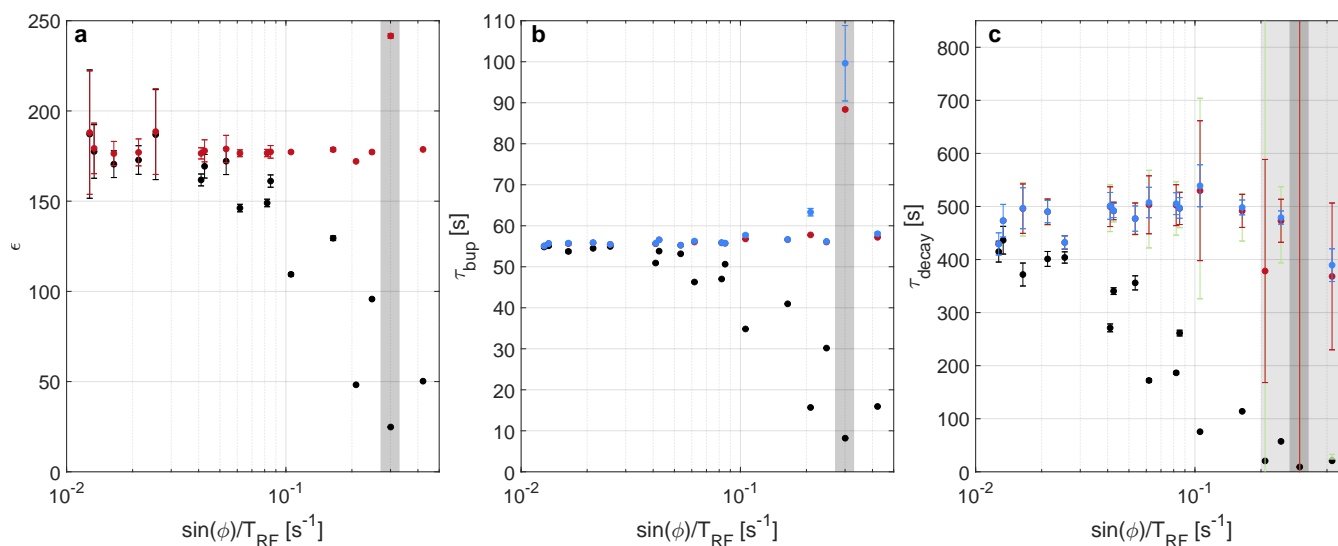


Figure 5. Experimental parameters - enhancement (a), build-up (b) and decay times (c) - with and without correction for the different experiments with TEMPO in the natural abundance sample as shown in Tab. 3, ordered by the relaxation due to RF pulsing ($\sin(\theta)/T_R$). Black refers to the uncorrected data, red to the iterative correction, blue and green to the CC-correction and $1/\cos^n$ correction, respectively. The uncertainties extracted from the 95% fit intervals of the respective build-up and decay measurements are often smaller than the symbol.



	θ	T_R	$\sin(\theta)/T_R$	ϵ		τ_{bup}	τ_{bup}	τ_{bup}	τ_{decay}	τ_{decay}	τ_{decay}	τ_{decay}
	[°]	[s]	[10^{-2} s^{-1}]	uncorr.	iter. corr.	uncorr.	iter. corr.	CC	uncorr.	iter. corr.	CC	cos. corr.
1	0.7	1	1.3	187	188	55	55	55	415	429	429	429
2	0.7	0.5	2.5	187	189	55	55	55	404	432	432	432
3	1.5	2	1.3	178	179	55	56	56	436	473	473	473
4	1.5	0.5	5.3	172	179	53	55	55	356	477	477	476
5	2.4	2	2.1	173	177	54	56	56	401	490	490	489
6	2.4	1	4.3	169	178	54	57	57	340	492	492	489
7	2.4	0.5	8.5	161	177	51	56	56	261	496	497	494
8	4.7	5	1.6	171	176	54	56	56	372	496	497	495
9	4.7	2	4.1	162	176	51	56	56	271	500	501	497
10	4.7	1	8.2	149	177	47	56	56	187	502	505	496
11	4.7	0.5	16	129	179	41	57	57	114	492	498	479
12	7.1	2	6.2	146	177	46	56	56	172	503	507	495
13	7.1	0.5	25	96	177	30	56	56	57	473	479	465
14	12.2	2	11	109	177	35	57	58	76	530	539	515
15	12.2	0.5	42	50	179	16	57	58	21	368	389	29
16	24.7	2	21	48	172	16	58	63	21	378	1240	$1.5 \cdot 10^6$
17	36.9	2	30	25	242	8	88	100	9	2604	-367	$8.2 \cdot 10^4$

Table 3. Overview of different experimental flip angles and correction methods with TEMPO in a natural abundance $\text{H}_2\text{O}/$ glycerol sample. The iterative correction refers to the above introduced correction algorithm. The label "CC" refers to Eq. (9). For the decay, we compare these two with a simple $1/\cos^n$ correction. ϵ refers to the DNP enhancement. $\sin(\theta)/T_R$ can be interpreted as a relaxation rate due to RF pulsing. This data is summarized in Fig. 5.

depend strongest on the flip angle used and only weakly on the SNR as the methods become inaccurate for similar flip angles in the low SNR simulations and high SNR experiments. Therefore, it appears likely that the (iterative, self-consistent and CC) corrections would perform well for samples with low experimental SNR although we did not show this experimentally within
 210 this work.

In our analysis of the experimental data, we included an offset for the build-up and decay fit as a free fitting parameter. This was necessary as the first data point of the acquisition is acquired with some delay due to the time the spectrometer needs to load the data acquisition sequence after the separate saturation sequence (the loading takes a few seconds). This leads to a higher polarization of the first acquired data point as can be seen in Fig. 3a (for the shown build-up simulation, the initial
 215 polarization of the first data point was set to the first data acquisition point). Including this offset leads to very accurate (build-



up) fits and with it of the RF correction. Including the offsets increases stability of the fits and corrections at the expense of larger uncertainties in the fitted parameters given the additional unknown.

220 The measured enhancements depend on a thermal equilibrium measurement. Since the presented results compare the relative differences between measurements, the uncertainty of the thermal equilibrium measurement does not affect the performance of the corrections. Furthermore, the conversion of the measured signal into enhancements depends on the flip angle. Uncertainty in the flip angles was not included in the calculation of the error bars. Another experimental complication causing differences between the experiments are drifts in the microwave power and cryostat as well as sample temperature. However, these are difficult to quantify but can be observed experimentally.

7 Conclusions

225 We simulated and demonstrated experimentally the ability to correct for the effects of readout RF pulses in dynamic nuclear polarization. The iterative correction approach allows to correct build-ups (enhancement, build-up time constant and individual data points) up to 25° and decays up to 12° pulses.

230 The experiments are supported by modelling relying on a first-order differential equation which offers insights into the relationships between the experimental parameters and can quantify the balance between hyperpolarization injection and relaxation in experiments, eventually leading to a better understanding of the processes limiting the achievable hyperpolarization.

Code and data availability. All data and MATLAB scripts can be found under DOI:10.3929/ethz-b-000606640. A MATLAB script to perform the experimental flip angle corrections can be found under <https://gitlab.ethz.ch/gvwitte/rfcorrection>.

Author contributions. All authors designed the research. GvW developed the model and performed the simulations. GvW performed experiments and analysis. All authors discussed the results and were involved in writing the manuscript.

235 *Competing interests.* One of the (co-)authors (ME) is an executive editor and member of the editorial board of Magnetic Resonance. The peer-review process was guided by an independent editor, and the authors also have no other competing interests to declare.

Acknowledgements. We thank Aaron Himmler for help with the experiments and Gian-Marco Camenisch for help with sample preparation.

ME acknowledges support by the Schweizerischer Nationalfonds zur Förderung der Wissenschaftlichen Forschung (grant no. 200020_188988). Financial support of the Horizon 2020 FETFLAG MetaboliQs grant is gratefully acknowledged.



240 References

- Adams, R. W., Aguilar, J. A., Atkinson, K. D., Cowley, M. J., Elliott, P. I. P., Duckett, S. B., Green, G. G. R., Khazal, i. G., Lopez-Serrano, J., and Williamson, D. C.: Reversible Interactions with para-Hydrogen Enhance NMR Sensitivity by Polarization Transfer, *Science*, 323, 1708–1711, 2009.
- Ajoy, A., Liu, K., Nazaryan, R., Lv, X., Zangara, P. R., Safvati, B., Wang, G., Arnold, D., Li, G., Lin, A., Raghavan, P., Druga, E., Dhomkar, S., Pagliero, D., Reimer, J. A., Suter, D., Pines, A., and Meriles, C. A.: Orientation-independent room temperature optical ^{13}C hyperpolarization in powdered diamond, *Science Advances*, 4, 1–8, <https://doi.org/10.1126/sciadv.aar5492>, 2018.
- 245 Akbey, Ü., Trent Franks, W., Linden, A., Orwick-Rydmark, M., Lange, S., and Oschkinat, H.: Hyperpolarization methods in NMR spectroscopy, vol. 338, <https://doi.org/10.1007/128-2013-436>, 2013.
- Ardenkjær-Larsen, J. H., Fridlund, B., Gram, A., Hansson, G., Hansson, L., Lerche, M. H., Servin, R., Thaning, M., and Golman, K.: Increase in signal-to-noise ratio of $>10,000$ times in liquid-state NMR, *Proceedings of the National Academy of Sciences of the United States of America*, 100, 10 158–10 163, <https://doi.org/10.1073/pnas.1733835100>, 2003.
- 250 Ardenkjaer-Larsen, J. H., Boebinger, G. S., Comment, A., Duckett, S., Edison, A. S., Engelke, F., Griesinger, C., Griffin, R. G., Hilty, C., Maeda, H., Parigi, G., Prisner, T., Ravera, E., Van Bentum, J., Vega, S., Webb, A., Luchinat, C., Schwalbe, H., and Frydman, L.: Facing and Overcoming Sensitivity Challenges in Biomolecular NMR Spectroscopy, *Angewandte Chemie - International Edition*, 54, 9162–9185, <https://doi.org/10.1002/anie.201410653>, 2015.
- 255 Broadway, D. A., Tetienne, J. P., Stacey, A., Wood, J. D., Simpson, D. A., Hall, L. T., and Hollenberg, L. C.: Quantum probe hyperpolarisation of molecular nuclear spins, *Nature Communications*, 9, 1–8, <https://doi.org/10.1038/s41467-018-03578-1>, 2018.
- Capozzi, A., Cheng, T., Boero, G., Roussel, C., and Comment, A.: Thermal annihilation of photo-induced radicals following dynamic nuclear polarization to produce transportable frozen hyperpolarized ^{13}C -substrates, *Nature Communications*, 8, 1–7, <https://doi.org/10.1038/ncomms15757>, 2017.
- 260 Chessari, A., Cousin, S. F., Jannin, S., and Stern, Q.: The role of electron polarization on nuclear spin diffusion, <http://arxiv.org/abs/2206.14771>, 2022.
- Corzilius, B.: High-field dynamic nuclear polarization, *Annual Review of Physical Chemistry*, 71, 143–170, <https://doi.org/10.1146/annurev-physchem-071119-040222>, 2020.
- 265 Corzilius, B., Smith, A. A., and Griffin, R. G.: Solid effect in magic angle spinning dynamic nuclear polarization, *The Journal of Chemical Physics*, 054201, 2012.
- Dementyev, A. E., Cory, D. G., and Ramanathan, C.: Dynamic nuclear polarization in silicon microparticles, *Physical Review Letters*, 100, 1–4, <https://doi.org/10.1103/PhysRevLett.100.127601>, 2008.
- Eichhorn, T. R., Parker, A. J., Josten, F., Müller, C., Scheuer, J., Steiner, J. M., Gierse, M., Handwerker, J., Keim, M., Lucas, S., Qureshi, M. U., Marshall, A., Salhov, A., Quan, Y., Binder, J., Jahnke, K. D., Neumann, P., Knecht, S., Blanchard, J. W., Plenio, M. B., Jelezko, F., Emsley, L., Vassiliou, C. C., Haulte, P., and Schwartz, I.: Hyperpolarized Solution-State NMR Spectroscopy with Optically Polarized Crystals, *Journal of the American Chemical Society*, 144, 2511–2519, <https://doi.org/10.1021/jacs.1c09119>, 2022.
- 270 Himmler, A., Albannay, M. M., von Witte, G., Kozerke, S., and Ernst, M.: Electroplated waveguides to enhance DNP and EPR spectra of silicon and diamond particles, *Magnetic Resonance*, 3, 203–209, 2022.



- 275 Hope, M. A., Björgvinsdóttir, S., Halat, D. M., Menzildjian, G., Wang, Z., Zhang, B., Macmanus-Driscoll, J. L., Lesage, A., Lelli, M., Emsley, L., and Grey, C. P.: Endogenous ^{17}O Dynamic Nuclear Polarization of Gd-Doped CeO_2 from 100 to 370 K, *Journal of Physical Chemistry C*, 125, 18 799–18 809, <https://doi.org/10.1021/acs.jpcc.1c04479>, 2021.
- Jähnig, F., Kwiatkowski, G., Däpp, A., Hunkeler, A., Meier, B. H., Kozerke, S., and Ernst, M.: Dissolution DNP using trityl radicals at 7 T field, *Physical Chemistry Chemical Physics*, 19, 19 196–19 204, <https://doi.org/10.1039/c7cp03633g>, 2017.
- 280 Jähnig, F., Himmler, A., Kwiatkowski, G., Däpp, A., Hunkeler, A., Kozerke, S., and Ernst, M.: A spin-thermodynamic approach to characterize spin dynamics in TEMPO-based samples for dissolution DNP at 7-T field, *Journal of Magnetic Resonance*, 303, 91–104, <https://doi.org/10.1016/j.jmr.2019.04.012>, 2019.
- Jardón-Álvarez, D., Reuveni, G., Harchol, A., and Leskes, M.: Enabling Natural Abundance ^{17}O Solid-State NMR by Direct Polarization from Paramagnetic Metal Ions, *Journal of Physical Chemistry Letters*, 11, 5439–5445, <https://doi.org/10.1021/acs.jpcclett.0c01527>, 2020.
- 285 King, J. P., Jeong, K., Vassiliou, C. C., Shin, C. S., Page, R. H., Avalos, C. E., Wang, H. J., and Pines, A.: Room-temperature in situ nuclear spin hyperpolarization from optically pumped nitrogen vacancy centres in diamond, *Nature Communications*, 6, 1–5, <https://doi.org/10.1038/ncomms9965>, 2015.
- Kovtunov, K. V., Pokochueva, E. V., Salnikov, O. G., Cousin, S. F., Kurzbach, D., Vuichoud, B., Jannin, S., Chekmenev, E. Y., Goodson, B. M., Barskiy, D. A., and Koptyug, I. V.: Hyperpolarized NMR Spectroscopy: d-DNP, PHIP, and SABRE Techniques, *Chemistry - An Asian Journal*, 13, 1857–1871, <https://doi.org/10.1002/asia.201800551>, 2018.
- 290 Kwiatkowski, G., Jähnig, F., Steinhauser, J., Wespi, P., Ernst, M., and Kozerke, S.: Direct hyperpolarization of micro- and nanodiamonds for bioimaging applications – Considerations on particle size, functionalization and polarization loss, *Journal of Magnetic Resonance*, 286, 42–51, <https://doi.org/10.1016/j.jmr.2017.11.007>, 2018a.
- Kwiatkowski, G., Polyhach, Y., Jähnig, F., Shiroka, T., Starsich, F. H., Ernst, M., and Kozerke, S.: Exploiting Endogenous Surface Defects for Dynamic Nuclear Polarization of Silicon Micro- and Nanoparticles, *Journal of Physical Chemistry C*, 122, 25 668–25 680, <https://doi.org/10.1021/acs.jpcc.8b08926>, 2018b.
- 295 Leavesley, A., Jain, S., Kamniker, I., Zhang, H., Rajca, S., Rajca, A., and Han, S.: Maximizing NMR signal per unit time by facilitating the e-e-n cross effect DNP rate, *Physical Chemistry Chemical Physics*, 20, 27 646–27 657, <https://doi.org/10.1039/c8cp04909b>, 2018.
- Miyayoshi, K., Segawa, T. F., Takeda, K., Ohki, I., Onoda, S., Ohshima, T., Abe, H., Takashima, H., Takeuchi, S., Shames, A. I., Morita, K., Wang, Y., So, F. T., Terada, D., Igarashi, R., Kagawa, A., Kitagawa, M., Mizuochi, N., Shirakawa, M., and Negoro, M.: Room-temperature hyperpolarization of polycrystalline samples with optically polarized triplet electrons: pentacene or nitrogen-vacancy center in diamond?, *Magnetic Resonance*, 2, 33–48, <https://doi.org/10.5194/mr-2-33-2021>, 2021.
- 300 Natterer, J. and Bargon, J.: Para-Hydrogen Induced Polarization (PHIP), *Progress in Nuclear Magnetic Resonance Spectroscopy*, 31, 293–315, 1997.
- 305 Ni, Q. Z., Daviso, E., Can, T. V., Markhasin, E., Jawla, S. K., Swager, T. M., Temkin, R. J., Herzfeld, J., and Griffin, R. G.: High frequency dynamic nuclear polarization, *Accounts of Chemical Research*, 46, 1933–1941, <https://doi.org/10.1021/ar300348n>, 2013.
- Prisco, N. A., Pinon, A. C., Emsley, L., and Chmelka, B. F.: Scaling analyses for hyperpolarization transfer across a spin-diffusion barrier and into bulk solid media, *Physical Chemistry Chemical Physics*, 23, 1006–1020, <https://doi.org/10.1039/d0cp03195j>, 2021.
- Rej, E., Gaebel, T., Boele, T., Waddington, D. E., and Reilly, D. J.: Hyperpolarized nanodiamond with long spin-relaxation times, *Nature Communications*, 6, <https://doi.org/10.1038/ncomms9459>, 2015.
- 310 Shimon, D., Cantwell, K. A., Joseph, L., Williams, E. Q., Peng, Z., Takahashi, S., and Ramanathan, C.: Large Room Temperature Bulk DNP of ^{13}C via P1 Centers in Diamond, *Journal of Physical Chemistry C*, 126, 17 777–17 787, <http://arxiv.org/abs/2207.11961>, 2022.



- Smith, A. A., Corzilius, B., Barnes, A. B., Maly, T., and Griffin, R. G.: Solid effect dynamic nuclear polarization and polarization pathways, *Journal of Chemical Physics*, 136, <https://doi.org/10.1063/1.3670019>, 2012.
- 315 Stern, Q., Cousin, S. F., Mentink-Vigier, F., Pinon, A. C., Elliott, S. J., Cala, O., and Jannin, S.: Direct observation of hyperpolarization breaking through the spin diffusion barrier, *Science Advances*, 7, 1–14, <https://doi.org/10.1126/sciadv.abf5735>, 2021.
- Tan, K. O., Mardini, M., Yang, C., Ardenkjær-Larsen, J. H., and Griffin, R. G.: Three-spin solid effect and the spin diffusion barrier in amorphous solids, *Science Advances*, 5, 1–8, <https://doi.org/10.1126/sciadv.aax2743>, 2019.
- 320 Tateishi, K., Negoro, M., Nishida, S., Kagawa, A., Morita, Y., and Kitagawa, M.: Room temperature hyperpolarization of nuclear spins in bulk, *Proceedings of the National Academy of Sciences of the United States of America*, 111, 7527–7530, <https://doi.org/10.1073/pnas.1315778111>, 2014.
- Walker, T. G. and Happer, W.: Spin-exchange optical pumping of noble-gas nuclei Thad, *Reviews of Modern Physics*, 69, 629–642, <https://doi.org/10.1109/JSEN.2021.3086263>, 1997.
- 325 Wenckebach, W. T., Capozzi, A., Patel, S., and Ardenkjær-Larsen, J. H.: Direct measurement of the triple spin flip rate in dynamic nuclear polarization, *Journal of Magnetic Resonance*, 327, <https://doi.org/10.1016/j.jmr.2021.106982>, 2021.
- Wittmann, J. J., Eckardt, M., Harneit, W., and Corzilius, B.: Electron-driven spin diffusion supports crossing the diffusion barrier in MAS DNP, *Physical Chemistry Chemical Physics*, 20, 11 418–11 429, <https://doi.org/10.1039/c8cp00265g>, 2018.
- Yoon, D., Soundararajan, M., Sekatski, S., Genoud, J., Alberti, S., and Ansermet, J. P.: High-Field ¹³C Dynamic Nuclear Polarization in Nanodiamond, *Journal of Physical Chemistry C*, 123, 21 237–21 243, <https://doi.org/10.1021/acs.jpcc.9b04110>, 2019.